Two-dimensional magnetic correlations and partial long-range order in geometrically frustrated CaOFeS with triangle lattice of Fe ions

S. F. Jin,[1] Q. Huang,[2] Z. P. Lin,[1] Z. L. Li,[1] X. Z. Wu,[1] T. P. Ying,[1] G. Wang,[1] and X. L. Chen[1,3,*]

[1]*Research & Development Center for Functional Crystals, Beijing National Laboratory for Condensed Matter Physics, Institute of Physics, Chinese Academy of Sciences, Beijing 100190, China*

[2]*NIST Center for Neutron Research, National Institute of Standards and Technology, Gaithersburg, Maryland 20899, USA*

[3]*Collaborative Innovation Center of Quantum Matter, Beijing 100190, China*

(Received 7 January 2015; revised manuscript received 16 February 2015; published 18 March 2015)

We report the results on the structure, transport, and magnetic properties of a layered oxysulfide CaOFeS with a stacked triangle lattice of Fe ions. The susceptibility data show a broad maximum near 120 K, indicating the existence of two-dimensional (2D) short-range ordering in this compound. Features associated with long-range antiferromagnetic (AFM) phase transition are seen below 40 K. Meanwhile, a very small heat-capacity anomaly is detected around 35 K, and most of the measured magnetic entropy is lost during the 2D ordering process. Both crystal and magnetic structures were studied by neutron powder diffraction at 300, 125, 40, and 6 K. The structure was refined based on space group $P6_3mc$ with $a = 3.759\ 98(4)$ and $c = 11.383\ 51(16)$ Å at ambient temperature. Low-temperature diffraction reveals 2D magnetic correlations between Fe moments without showing significant structural distortion. Warren peak shape analysis of the neutron-diffraction data at 2θ near 18° is employed to characterize the correlation length in the 2D magnetic state with lowering temperature. The geometrically frustrated compound is found to gradually condense into a partial long-range ordered state with AFM coupled Fe layers between 40.6 and 26 K. The resulting partially ordered magnetic structure is a *G*-type Ising AFM with a propagation vector of $\mathbf{k} = (1/2,1/2,0)$ and an ordered magnetic moment of $2.59(3)\mu_B$/Fe along c at 6 K.

DOI: 10.1103/PhysRevB.91.094420 PACS number(s): 75.25.−j, 75.30.Cr, 75.40.−s, 74.62.Bf

I. INTRODUCTION

The antiferromagnetism occurring in certain lattice symmetries results in phenomena known broadly as geometrical frustration [1]. Geometrically frustrated magnets are fascinating materials displaying a rich variety of physical states. In these systems, magnetic moments interact by exchange, but no long-range magnetic structure is able to satisfy all antiferromagnetic (AFM) interactions simultaneously. Sufficiently strong competition can lead to new physics that is manifested by the appearance of noncollinear ordering, novel critical exponents, rich phase diagrams, or an absence of long-range order at low temperatures [2,3].

Many systems exhibit competing interactions, that is, interactions that do not all favor the same ordered state. One of the typical frustration effects may be seen in the triangular lattice antiferromagnetic (TLA) system. Considering the effects of frustration in the simplest stacked TLA systems, a majority of the previous research work involves one of three crystal structures, i.e., the ABX_3, BX_2 metal halides, and ABO_2 compounds (where A is an alkali metal, B is a transition metal, and X is a halogen atom) [4]. In ABX_3 compounds, there are chains of magnetic B atoms along the z direction coupled by superexchange interactions through three equivalent anions X. The magnitude of the interplanar interactions J is typically two to three orders of magnitude greater than intraplanar interactions J' so that at high temperatures the magnetic properties become quasione dimensional. In quasi-two-dimensional (2D) BX_2 and ABO_2 compounds, the strong superexchange coupling is intraplanar, and the ratio of the magnitude of the interactions is reversed.

It is well known that in a triangular lattice antiferromagnet in 2D with nearest-neighbor interaction only, no long-range order occurs at a finite temperature if the spin configuration is Ising type [5]. Frustration effects are more acute in Ising triangular antiferromagnets than in *XY* or Heisenberg systems. In the latter cases the frustration can be partially relieved by the formation of a spin triangle, and a typical spin ordering in a TLA is the 120° structure where the three spins align at 120° to each other in the basal plane with two types of chirality. Thus, few examples have been reported with properties that exhibit Ising antiferromagnets where spins are confined to directions parallel and antiparallel to z [4]. For instance, only the Hamiltonians in a cobalt member of ABX_3 have reported to be close to the Ising Hamiltonian [6]. However, in each case the unit cell is $\sqrt{3}a \times \sqrt{3}a$, and the arrangement states within the ab plane are either partially ordered or become ferrimagnetic [7,8]. Moreover, a neutron scattering by VI_2 indicates a collinear Ising structure, however, the results conflict with another measurement [2,9]. Therefore, it is of great interest to search for new layered TLA compounds that show collinear Ising spin configurations and investigate the underlying frustration effects.

Meanwhile, strongly correlated layered transition-metal compounds are one of the most active research topics in both fundamental and applied condensed-matter physics. Particularly, the discovery of layered iron oxypnictide [La(O,F)FeAs, 1111-type] superconductors with T_c up to 26 K has inspired worldwide interest on layered iron-based compounds [10]. The 1111-type oxychalcogenides then become a subject of current interest. Besides the oxychalcogenide R_eOCuC (R_e = rare earth and Bi, C = Se,S) serials [11,12], which are isostructural to LaOFeAs, some of the reported 1111 oxysulfides were found crystallized in interesting stacked triangular lattices, i.e., CaOMS (M = Zn [13,14],Fe [15]). Previously,

*Corresponding author: chenx29@iphy.ac.cn

the potential TLA compound CaOFeS was found always to coexist with excessive impurities, and further investigation on this compound was not possible [15].

Here, we report the phase pure synthesis and detailed physical properties of the layered TLA compound CaOFeS. To characterize this material, we performed a number of measurements including powder neutron diffraction, electrical transport, heat capacity, and magnetization. Our results suggest that CaOFeS is a frustrated magnetic insulator with a stacked triangle lattice of Fe moments. The susceptibility data reveal that 2D short-range ordering exists in CaOFeS below room temperature, followed by a 2D short-range to three-dimensional (3D) long-range AFM ordering phase transition at 40 K. Instead of a significant magnetic specific-heat peak, only a very small peak is detected near 40 K in the heat-capacity data, indicating that the magnetic entropy is primarily lost in the 2D ordering process. The analysis of the neutron powder-diffraction data shows the compound has planar magnetic correlations that condense into a partial long-range ordered state with a very rare *G*-type triangle AFM configuration coexisting with the short-range correlations. The neutron spectra also revealed the 2D to partial 3D long-range AFM transition between 40.6 and 26 K.

II. EXPERIMENTAL METHODS

Polycrystalline samples of CaOFeS were prepared by the reaction of CaO (99.9%, Alfa-Aesar, heated to 1000 °C prior to use), S (99.999%, Alfa-Aesar), and Fe (99.9%, Shiny) powders in a molar ratio of 1:1:1. These reagents were intimately ground together using an agate pestle and mortar and placed in an alumina crucible. Al powder (10% per formula) was placed in a second alumina crucible to act as an oxygen getter (forming Al_2O_3 during the reaction, and samples without reducing agents were found containing a significant amount of oxygen-rich impurity phases). These two crucibles were placed inside a quartz tube which was evacuated, sealed, and then heated slowly to 800 °C and held at this reaction temperature for 48 h. The sample was then furnace cooled to room temperature. CaOFeS thus prepared is shiny black polycrystalline. Polycrystalline samples of CaOZnS were prepared by the reaction of CaS (99.9%, Alfa-Aesar) and ZnO (Sinopharm, 99.9%) powders in a molar ratio of 1:1. The reagents were evacuated and heated to 1000 °C and held at this reaction temperature for 36 h.

Neutron powder-diffraction measurements were performed on the high-resolution powder diffractometer BT1 equipped with a closed cycle refrigerator system at the Center for Neutron Research of the National Institute of Standards and Technology. Approximately 7 g of finely ground CaOFeS powder was used in the measurements. The sample was loaded into vanadium containers in a He glovebox, and the can was sealed using indium gaskets. The patterns were measured at 300 K using a Cu (3 1 1) monochromator with a neutron wavelength of 1.5403 Å and at 125, 40, and 6 K using a Ge (3 1 1) monochromator with a neutron wavelength of 2.0783 Å. Rietveld refinements on neutron-diffraction patterns were carried out using the GSAS program suite. The background was fitted by a 12-coefficient polynomial function.

dc magnetization $M(T)$ was measured in a Quantum Design (QD) physical properties measurement system using finely grounded powders. The $M(T)$ data were collected on warming from 10 to 300 K after the sample was first zero-field cooled (ZFC) and then field cooled (FC) from 300 to 10 K, respectively. The susceptibility was calculated as $\chi = M(T)/H$. No correction for sample holder or core diamagnetism was employed in the magnetization data presented because these temperature-independent terms are very small. Temperature-dependent heat capacities were measured in a QD physical properties measurement system using the relaxation technique at zero field. Resistivities were measured in a QD physical properties measurement system using the standard four-probe configuration. The samples were cut into bars, and four platinum wires were attached on the bar by silver paste.

III. EXPERIMENTAL RESULTS AND DISCUSSIONS

A. Crystal structure

From the Rietveld quantitative analyses of the room-temperature neutron-diffraction patterns, our CaOFeS sample is estimated to contain 97.0% of the CaOFeS phase in mass fraction and impurity phases of Fe (1.4% mass) and CaS (1.6% mass). The room-temperature structure of CaOFeS is noncentrosymmetric and crystallizes in a polar space group $P6_3mc$ adopted by a previously reported compound CaOZnS [13]. As shown in Table I, the structural parameters obtained after refinement produced an excellent fit to the diffraction pattern with $R_p = 3.39\%$, $wR_p = 4.98\%$, justifying the validity of the results. The crystal structure consists of alternately stacked hexagonal layers of CaO and FeS (Fig. 1), and the Fe atom is tetrahedrally coordinated by three S atoms and one O atom in a neighboring CaO layer [Fig. 1(a)]. The three Fe-S bond lengths are 2.3975(15) Å, which is more than 0.5 Å larger than the Fe-O bond length, resulting in

TABLE I. Room-temperature structure details of CaOFeS. U_{iso} is the isotropic Debye-Waller factors; R_p and wR_p are the agreement R factors.

	CaOFeS	
Space group (No. 186)		$P63mc$
a(Å)	3.75998(4)	
c(Å)	11.3835(2)	
V(Å^3)	139.373(3)	
Atomic positions		$U_{iso} \times 100$ (Å)
Ca (2b)	1/3,2/3,0.2686(2)	1.28(5)
O (2a)	0,0,0.3356(1)	1.10(3)
Fe (2a)	0,0,0	1.61(2)
S (2b)	2/3,1/3,0.0894(3)	1.40(8)
Coordination		
$d_{Fe\text{-}O}$(Å)	1.871(1) ×1	
$d_{Fe\text{-}S}$(Å)	2.398(2) ×3	
$a_{O\text{-}Fe\text{-}S}$(deg)	115.12(7)	
$a_{S\text{-}Fe\text{-}S}$(deg)	103.28(6)	
Agreement indices overall		
		$R_p = 0.0339$
		$wR_p = 0.0498$

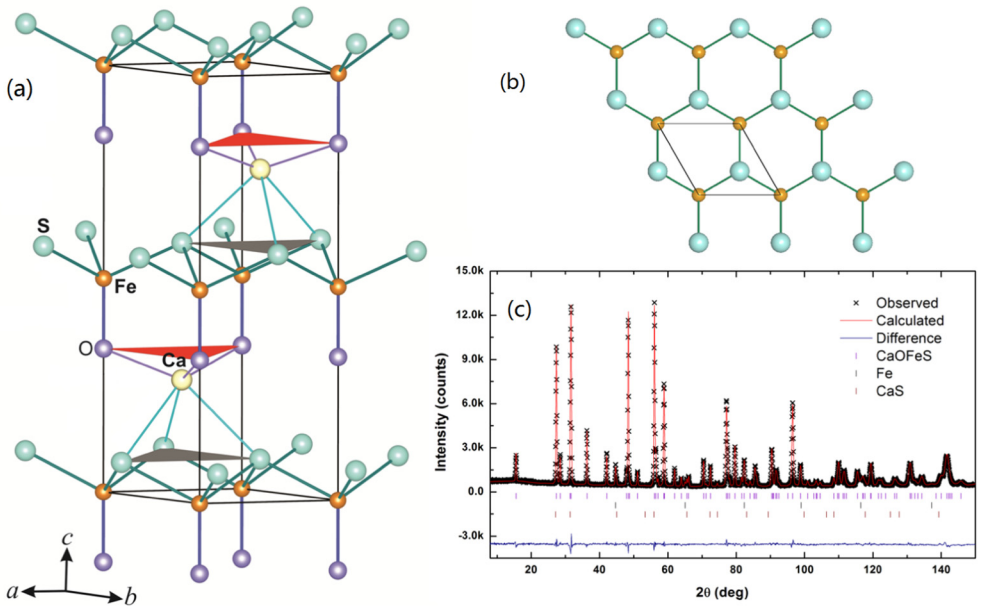

FIG. 1. (Color online) (a) Room-temperature crystal structure of CaOFeS, (b) coordination environment of the $\infty[FeOS_3]$ plane, (c) powder neutron diffraction and result of Rietveld refinement of the CaOFeS sample at 300 K.

a highly distorted FeS_3O tetrahedron. The layers of FeS_3O tetrahedra aligned with their Fe-O bond parallel to the c axis and linked at their S vertices result in a stacked triangle lattice of Fe ions [Fig. 1(b)]. The nearest intralayer Fe-Fe distance is $d1 = 3.759\ 88(2)$ Å(a) whereas the nearest interlayer Fe-Fe distance is $d2 = 5.691\ 76(8)$ Å$(c/2)$. The ratio of $d2/d1$ is about 1.51. The selected bond lengths and angles are also given in Table I. It should be noted that the most striking feature in CaOFeS is the formation of a FeS_3O layer, which is not common in oxyphosphates of alkaline earths and lanthanides, such as LaOFeAs. In the LaOFeAs type of compounds, LaO and FeAs layers are not connected by chemical bonds. In comparison, the iron atom in CaOFeS is presumably bonded to oxygen in a competitive manner with calcium, resulting in the highly distorted FeS_3O coordination, which bridges the CaO and FeS layers.

B. Magnetic susceptibility, heat capacity, and electrical resistivity

The temperature-dependent susceptibility is presented in Fig. 2. Both ZFC warming and FC warming data are shown. No Curie-Weiss behavior is observed up to the highest temperature measured 300 K. Instead, a broad maximum near $T_{max} = 120$ K with no bifurcation between FC and ZFC data is detected, which suggests the presence of low-dimensional short-range spin correlations among Fe ions at high temperatures [16]. For a highly two-dimensional system, T_{max} is proportional to the nearest-neighbor spin exchange [17,18], i.e., the measure of the intralayer coupling. The previously reported oxychalcogenide compound $La_2O_3Fe_2Se_2$ has a similar $T_{max} = 120$ K [19], meanwhile, the T_{max} values are up to 270 and 350 K for $La_2O_3Co_2Se_2$ and $La_2O_3Mn_2Se_2$, respectively [20,21]. At lower temperatures, the ZFC and FC data decrease gradually, and a bifurcation between ZFC and FC data appears below 40 K. For clarity, the magnetic susceptibility below 60 K is shown in the inset of Fig. 2. The ZFC data show continuous decreases in the susceptibility, featured by an anomaly between 20 and 30 K, a signature of successive AFM phase transitions. Meanwhile, the FC data show an upturn below 40 K instead of the continuous decrease seen in the ZFC data upon cooling, suggesting the presence of a ferromagnetic contribution to the susceptibility under a high cooling field. The bifurcation and anomaly appearing in the susceptibility are the occurrence of a partial AFM phase transition, see Sec. III C.

To further clarify the magnetic anomaly, we performed a heat-capacity measurement on the polycrystalline CaOFeS. Considering the susceptibility data show strong 2D correlations, the magnetic heat capacity may have similar broad features that easily mixed with the phonon contributions. Therefore, the heat capacity of a diamagnetic isostructural

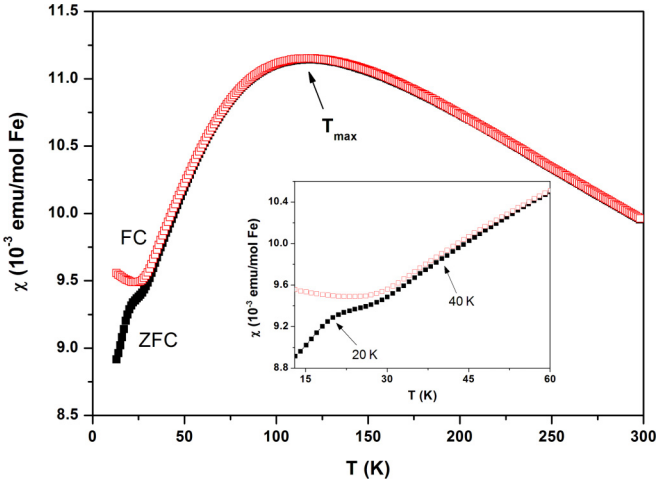

FIG. 2. (Color online) ZFC and FC $\chi(T)$ data taken in an applied field of 10 kOe. Inset: enlarged $\chi(T)$ data below 60 K.

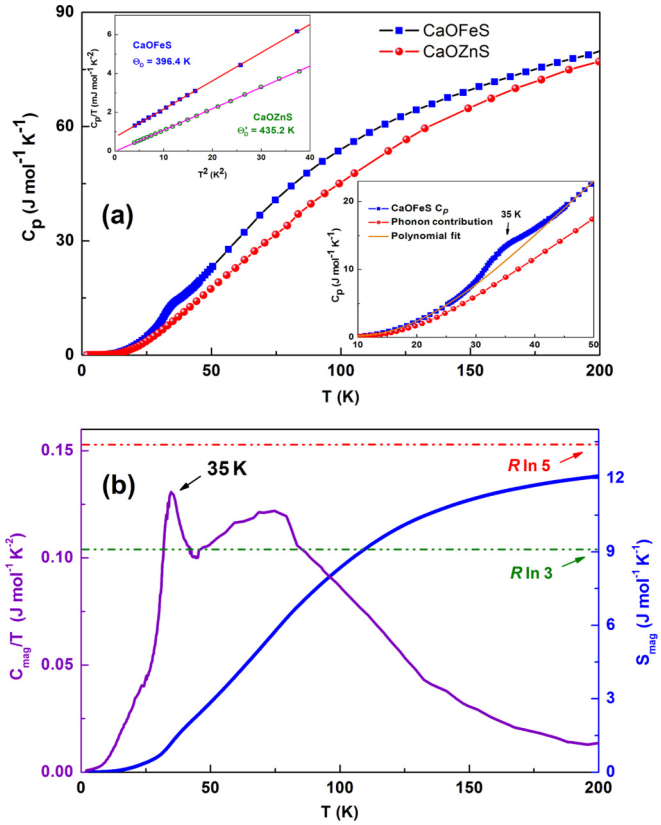

FIG. 3. (Color online) (a) Temperature dependence of specific heat for CaOFeS between 200 and 2 K; the heat capacity of a diamagnetic isostructural material CaOZnS is measured to account for the lattice component. Left inset: The low-temperature specific-heat data in the plot of C_p/T vs T [2]. The solid lines are fitted using formula $C_p/T = \beta T^2 + \alpha$; right inset: enlargement of the specific-heat data to emphasize a small peak contributed by magnetic entropy around 35 K; the orange curve represents a polynomial fit by neglecting this peak. (b) Temperature dependence of magnetic entropy and $C_{\rm mag}/T$ for CaOFeS, and the $C_{\rm mag}/T$ data show a very broad feature in the temperature range between 200 and 40 K and a relative sharp contribution to the magnetic entropy of ∼35 K.

material CaOZnS was measured to accurately account for the lattice component of CaOFeS. Figure 3(a) presents the $C_p(T)$ data for CaOFeS and CaOZnS measured from 200 to 2 K, respectively. After subtracting the phonon contribution ($C_{\rm ph}$) from the total specific heat, the magnetic contribution ($C_{\rm mag}$) can be obtained [22]. As shown in Fig. 3(a), $C_{\rm mag}$ has a very broad feature in the measured temperature range and has already become significant at 200 K. Moreover, the $C_p(T)$ data of CaOFeS show a small maximum between 28 and 41 K [right inset of Fig. 3(a)]. The peak position is very close to the bifurcation temperature ($T_{\rm B} = 40$ K) at the $\chi(T)$ curve (inset of Fig. 2), suggesting that a long-range AFM ordering forms at this temperature. The magnetic entropy can be calculated using $S_{\rm mag}(T) = \int_0^T C_{\rm mag}/T\, dT$. In Fig. 3(b), we give the temperature dependence of $C_{\rm mag}/T$ and $S_{\rm mag}$. The derived $S_{\rm mag}$ increases gradually over the entire measured temperature range and reaches $S_{\rm mag} = 12.1$ J mol^{-1} K^{-1} when T is up to 200 K [Fig. 3(b)]. This value corresponds well with the expected values for Fe^{2+} ions with a high spin state (∼90.4% of R ln 5) in tetrahedral crystal fields and seems to rule out the low spin state (up to 132% of R ln 3). Meanwhile, the $C_{\rm mag}/T$ curve shows a very broad feature at higher temperatures that results from the 2D magnetic ordering. The 2D ordering releases a majority of magnetic entropy before it reaches a small sharp peak (∼35 K) that corresponds to long-range magnetic transition. Similarly, the very small $S_{\rm mag}$ at the $T_{\rm N}$ has been observed in previously reported highly 2D magnetic systems, e.g., $La_2O_3Mn_2Se_2$ [21]. It is noticed that the small value of $S_{\rm mag}$ is also observed in the parent materials of iron pnictide superconductors, which is mainly ascribed to the itinerancy of Fe ions. However, as shown below, CaOFeS is an insulator by transport measurement, and the small value of $S_{\rm mag}$ should then be mainly due to the 2D AFM order above $T_{\rm N}$(40 K). At low temperatures, the $C_p(T)$ curve of CaOFeS can be well fitted to a relation $\alpha T + \beta T$ [3] [inset of Fig. 3(a)], and the fitted value β is 0.14555mJ mol^{-1} K^{-4}. According to the formula $\Theta_{\rm D} = (12\pi^4 NR/5\beta)^{1/3}$, the Debye temperature is estimated to be $\Theta_{\rm D} = 396.4(2)$ K, consistent with what is expected for an oxysulfide of this type. In comparison with CaOZnS, the extra αT component of the CaOFeS sample could be either originated from the minor Fe impurities (1.4% mass) or originated from the remnant partial magnetic ordering states as discussed in Sec. III C.

The electrical resistivity of CaOFeS is shown in Fig. 4 from which an insulating ρ vs T dependence is clearly seen. At 300 K, the magnitude of resistivity is 30.9 Ω m. In the inset of Fig. 4, we show ρ vs $1/T$ in the logarithmic plot, and we found that the $\rho(T)$ curve does not follow well the Arrhenius law for thermally activated hopping, viz., $\rho(T) \propto \exp(\Delta/T)$. Instead, the data are better fitted to $\rho(T) \propto \exp[(D/T)^{1/4}]$, which is known as the 3D variable range hopping stemming from the random potential scattering contributed by large numbers of defects or disorders [23]. A similar phenomenon was also observed in $BaFe_2Se_2O$ [24] A rough estimate of activating energy $\Delta \sim 0.21(1)$ eV will be derived from the data 230–300 K, consistent with the black color of the compound, and

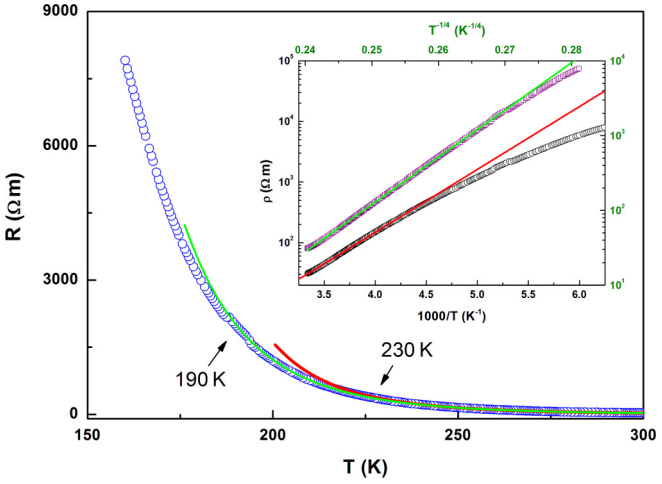

FIG. 4. (Color online) Temperature dependence of the resistivity $\rho(T)$ of the CaOFeS with $H = 0$. The inset shows the fitting results of $\rho(T)$ at zero field using a thermal activation model (red line) and a variable range hopping model (green line).

confirm that CaOFeS is a narrow gap insulator. Below 190 K, the resistivity data cannot be fitted by a simple model.

C. Magnetic structure

To determine the magnetic structure of CaOFeS, neutron powder-diffraction data were collected at $T =$ 6, 40, 125, and 300 K. Figure 5 shows the observed, calculated, and difference neutron-diffraction profiles below 125 K for CaOFeS where the magnetic ordering is gradually established. The patterns collected at 125 and 40 K can be fitted very well by a structural model based on CaOZnS in the space group $P6_3mc$. The agreement factor for refinement is wR_p of 0.041 and 0.043, indicating the high quality of the fit as does a comparison of the observed and calculated patterns [Figs. 5(a) and 5(b)]. Meanwhile, a broad diffracted intensity feature is found centered around 20° for the two patterns. This is clear evidence for the presence of short-range spin ordering at those temperatures, which is consistent with our susceptibility measurements. This broad feature is also observed in the $T =$ 6-K neutron spectrum and will be discussed below.

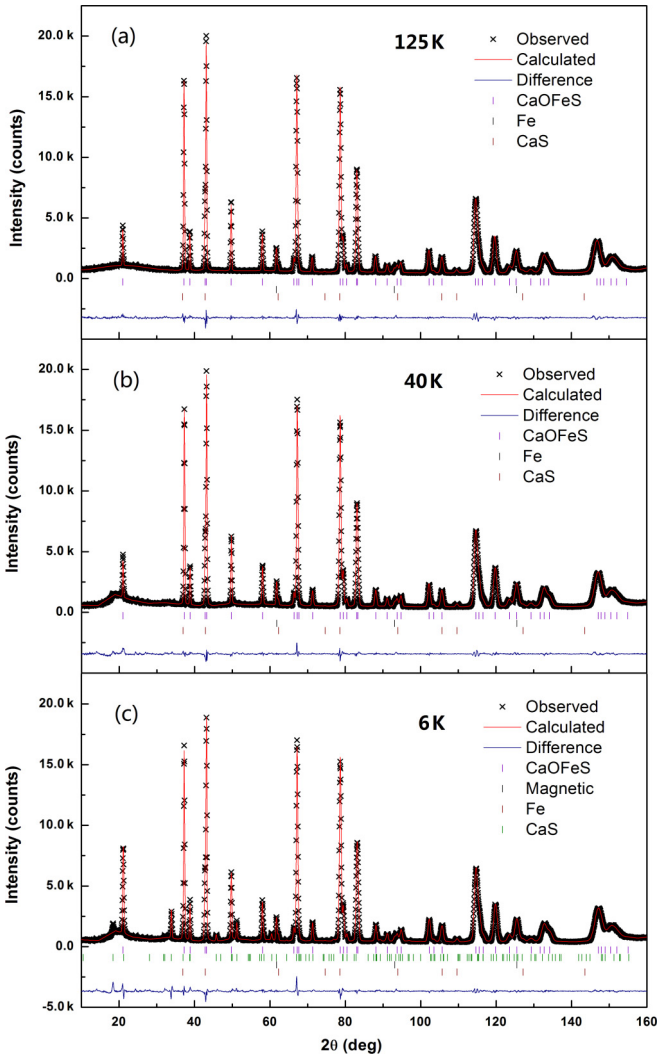

FIG. 5. (Color online) Neutron powder-diffraction pattern for CaOFeS taken at (a) 125 K, (b) 40 K, and (c) 6 K. Upper black cross: observed pattern; upper red curve: calculated pattern; tick marks: calculated peak positions; lower curve: difference between observed and calculated patterns. Magnetic stands for the magnetic Bragg peak.

TABLE II. Chemical and magnetic structure details of CaOFeS at $T =$ 125, 40, and 6 K. R_p and wR_p are the agreement R factors.

	T		
	125 K	40 K	6 K
Chemical structure			
a(Å)	3.75469(7)	3.75167(7)	3.75165(7)
c(Å)	11.3796(2)	11.3821(2)	11.3846(3)
V(Å^3)	138.933(6)	138.740(7)	138.769(7)
z-Ca	0.2663(2)	0.2661(2)	0.2665(2)
z-O	0.33498(8)	0.33492(8)	0.3347(1)
z-S	0.0898(3)	0.0895(3)	0.0900(3)
$d_{\text{Fe-O}}$(Å)	1.8779(9)	1.8790(9)	1.882(1)
$d_{\text{Fe-S}}$(Å)	2.397(1)	2.394(1)	2.396(2)
$a_{\text{O-Fe-S}}$(deg)	115.25(6)	115.19(7)	115.32(8)
$a_{\text{S-Fe-S}}$(deg)	103.13(8)	103.19(9)	103.04(9)
R_p	0.0326	0.0348	0.0392
wR_p	0.0410	0.0426	0.0500
Magnetic structure			
$M_Z(\mu_B)$			2.59(3)

The neutron-diffraction pattern measured at 6 K is presented in Fig. 5(c). A comparison of the spectra at 40 K [Fig. 5(b)] and 6 K between 20° and 60° reveals large extra peaks due to the 3D long-range AFM ordering at 6 K. Thus, a combined magnetic and crystal structure refinement was performed for the diffraction patterns collected at 6 K. The refined structural and magnetic parameters at 125, 40, and 6 K are summarized in Table II, and no structural phase transition is observed between 300 and 6 K. The temperature dependence of unit-cell parameters a and c values, the O-Fe-S and S-Fe-S bond angles, as well as the Fe-S and Fe-O bond lengths at the measured temperatures are plotted in Fig. 6. From 6 K to room temperature, the lattice constant a increases monotonically by 0.2%, whereas c first decreases from 11.3846(3) to 11.3796(3) Å at 125 K and then increases to 11.3835(2) Å at ambient temperature. Meanwhile, ∠O-Fe-S decreases slightly from 115.32(8)° to 115.12(7)°, whereas ∠S-Fe-S increases from 103.04(9)° to 103.28(6)°. The Fe-O bond length decreases monotonically from 1.8816(11) to 1.8709(11) Å, and the Fe-S bonds remain almost constant. No clear changes in the lattice constants, bond angles, and lengths accompany the 3D magnetic ordering.

The magnetic structure was determined from the neutron-diffraction pattern taken at 6 K. Magnetic symmetry analysis was performed by the BASIREPS program [25]. Together with the Rietveld structure refinement, the magnetic reflections, as shown in the Fig. 5(c), can be well fitted to a magnetic cell that has the twofold dimensions on the ab plane as the crystallographic cell with a magnetic propagation vector $\mathbf{k} = (1/2, 1/2, 0)$. The analysis shows CaOFeS has a G-type collinear AFM structure as shown in Fig. 7(a) with the ordered magnetic moment along the c direction. The intraplane antiferromagnets of CaOFeS have a rare triangular Ising type, and the ordered magnetic moment has an average value of

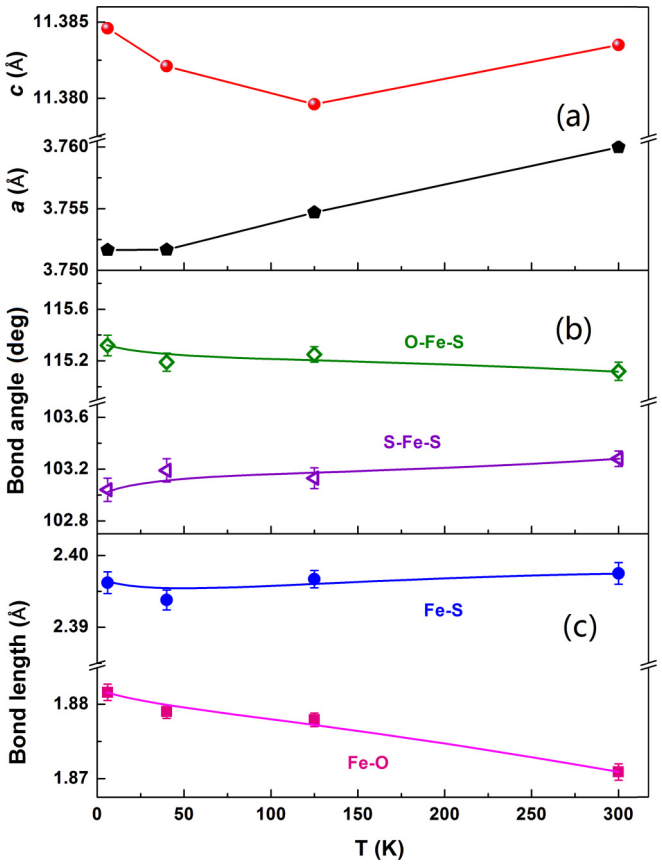

FIG. 6. (Color online) (a) Normalized lattice parameters a and c of CaOFeS vs temperature and (b) O-Fe-S and S-Fe-S vs T. (c) Fe-S and Fe-O bond lengths vs temperature, respectively.

$2.59(3)\mu_B$/Fe at 6 K where spins are confined to directions parallel and antiparallel to z. It should be noted that the spin state of Fe^{2+} in a quasitetrahedral site would be either $e^3t_2^3$ (nominally $S = 2$) for high spin or $e^4t_2^2(S = 1)$ for low spin. The observation of an ordered moment on Fe of $2.59(3)\mu_B$ would seem to rule out the low spin configuration, consistent with the measured magnetic specific heat. In the pnictide superconductors, Fe is regarded as largely itinerant, but that is clearly not the case here.

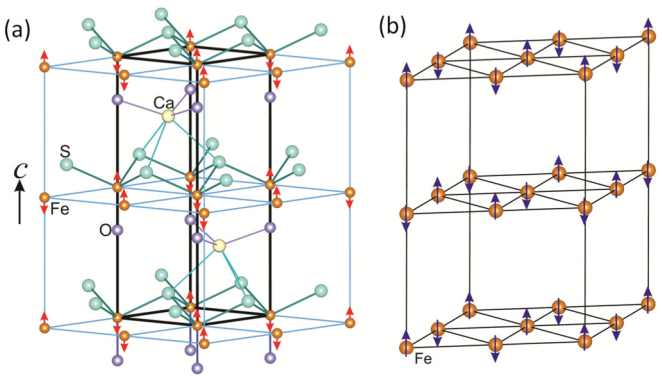

FIG. 7. (Color online) (a) Chemical and magnetic structures of CaOFeS at 6 K. (b) View of the Fe triangular coupling sheet; the magnetic structure is a G-type Ising AFM with a propagation vector of $\mathbf{k} = (1/2,1/2,0)$ and an ordered magnetic moment of $2.59(3)\mu_B$/Fe along c at 6 K.

The stacked triangular magnetic lattice is shown in Fig. 7(b), and the in-plane spins have sixfold symmetry. Two main magnetic interactions as shown in Fig. 7(a) have to be considered among the Fe^{2+} ions: the intraplane superexchange interaction through the Fe-S-Fe channel and the direct exchange interaction between interplane Fe-Fe. A Heisenberg-type antiferromagnetism with single-ion anisotropy can be described on the basis of the following Hamiltonian:

$$\hat{H} = J\sum_{i,j}^{\text{inter}} S_iS_j + J'\sum_{k,l}^{\text{intra}} S_kS_l + D\sum_i \left(S_i^z\right)^2 - g\mu_B H\sum_i S_i, \quad (1)$$

where S is a spin of the magnetic ion, J is the exchange integral along the c axis of the crystal, J' is the exchange integral in the perpendicular direction, and D is the anisotropy constant. The sign of anisotropy constant D influences the orientation of the spin plane relative to the crystal axes [4], i.e., the case of $D = 0$ corresponds to a pure Heisenberg system. If $D > 0$, the ground state in zero field favors spins confined to the xy plane, otherwise the anisotropy energy will be minimized for spins aligned perpendicular to the xy plane. According to a classic system proposed by Collins and Petrenko [4], the easy-axis spin arrangement in a system with the above Hamiltonian mainly depends on the relative strength of J' and D, and a collinear structure will be favored for higher $|D/J'|$ ratios, but only when $|D| = 3J'$ can the triangular structure collapse into a collinear spin structure along the c axis. However, the anisotropy is not large enough for this to happen in the previously investigated materials at low temperatures. Meanwhile, for typical quasi-2D triangular antiferromagnets, J' is generally stronger and often several orders bigger than J, e.g., neutron-scattering results for VCl_2 indicate $J' = 458(13)$ GHz and $J = 2.8(1)$ GHz. From the magnetic structure determined for CaOFeS where the nearest-neighbor Fe-Fe possesses collinear antiparallel spins, we infer that in CaOFeS the anisotropy constant $|D|$ is significantly larger than J' and thus leading to the stabilization of the strongly frustrated TLA Ising states.

The interplay between the spin-orbit interaction and the geometry distortion have been demonstrated to strongly affect the magnetocrystalline anisotropy, e.g., lattice distortion in $LaMnO_3$ is found crucial in stabilizing A-type AFM states [26]. For previously known Ising triangular antiferromagnets, e.g., the cobalt member of the ABX_3 compounds, geometrical distortions have also been observed. For instance, the cobalt cation lies in an octahedron of X anions with trigonal distortion. The strong crystal field splits the lowest-lying ^4F configuration so that a $^4T_1$ state has the lowest energy, which corresponds to Kramer's doublet with the moment lying parallel or antiparallel to the c axis [4]. For CaOFeS, the iron cation lies in a tetrahedron of three S and one O anions with significant distortion, and the crystal-field distortion may effectively increase anisotropy and hence split the lowest-lying Fe^{2+} configuration to force the moment easy axis.

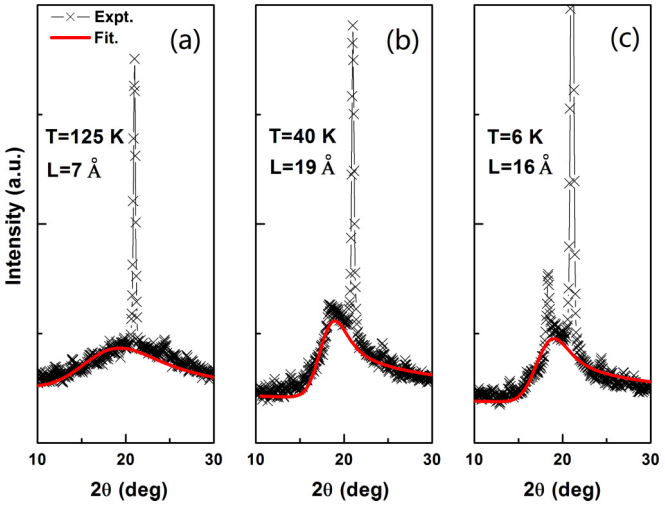

FIG. 8. (Color online) Enlarged neutron powder-diffraction pattern with the short-range ordering feature where the red solid line is the Warren line-shape fit.

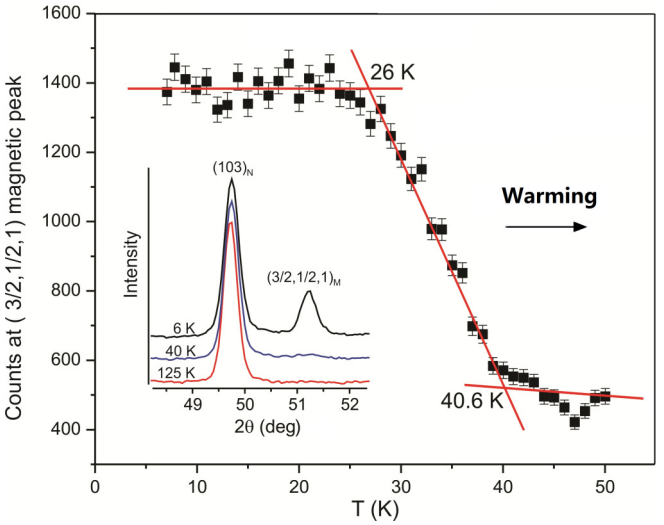

FIG. 9. (Color online) Temperature dependence of the intensity at the (3/2,1/2,1) magnetic Bragg peak in CaOFeS. The intensity data were obtained by measuring counts at the Bragg position of (3/2,1/2,1) magnetic peak vs T. Phase transition from a paramagnetic phase to a partial AFM phase was roughly estimated between 40.6 and 26 K. The inset shows the respective neutron data collected at 6, 40, and 125 K, respectively.

Comparison of the magnetic properties of all the members of the frustrated quasi-two-dimensional TLA systems is also of significant interest. Four BX_2 compounds have been previously studied: VCl_2 and VBr_2 are close to Heisenberg systems [2], meanwhile, although there is weak easy-axis anisotropy, the magnetic structure of VI_2 is not clear [4]. $MnBr_2$ has a complex magnetic structure which is not triangular in nature [27]. Among ABO_2 compounds, the magnetic properties of only three triangular antiferromagnets have been investigated in detail. $LiCrO_2$ and $CuCrO_2$ demonstrate 120° magnetic structure with weak easy-axis anisotropy [28,29], whereas $AgCrO_2$ has a slightly modulated 120° structure [30].

The neutron powder-diffraction data provide clear evidence for 2D short-range ordering in CaOFeS. Figure 8 shows the enlarged neutron-diffraction pattern between $2\theta = 16^\circ$ and 30° taken at $T = 125, 40$, and 6 K, respectively. At 125 K, a pronounced broad peak is found centered around $2\theta = 20^\circ$. This asymmetric peak, characterized by a relatively rapid increase at lower angles and a more gradual decrease at higher angles, becomes sharper in width and larger in magnitude at 40 K. After entering into the ordered state where the magnetic Bragg peaks are clearly detected at $2\theta = 22^\circ$ and 34°, the broad peak centered around 18° can still be observed but with a diminishing magnitude at 6 K. Interestingly, as shown in Fig. 9, the temperature dependence of the intensity of the (3/2,1/2,1) magnetic peak suggests the first magnetic ordering actually finished at 26 K. Then, the persisting signal from short-range correlations below 26 K proves the magnetic phase of CaOFeS is partially long-range ordered, similar to the recent observation in another strong geometrically frustrated Sr_2YRuO_6 in a quasi-fcc lattice [31]. The persisting asymmetric peak is of the Warren shape, which is the characteristic peak shape of 2D correlations and should be arising from layers that do not participate in the long-range ordering. The 2D correlation length can be obtained from Warren peak shape analysis [32], which can be expressed as

$$P'_{2\theta} = Km\frac{F^2(1+cos^2 2\theta)}{2(\sin\ \theta)^{3/2}}\left(\frac{L}{\sqrt{\pi}\lambda}\right)^{1/2} W(a), \qquad (2)$$

$$W(a) = \int_0^\infty \exp[-(x^2-a)^2]dx, \qquad (3)$$

with $a=(2\sqrt{\pi}L/\lambda)(\sin\ \theta - \sin\ \theta_0)$, L is the two-dimensional correlation length, K is a constant, m is the two-dimensional multiplicity, and F is the two-dimensional structure factor, which can be taken as a constant over small ranges of the angle. A linear background function is added to the Warren function in the fitting. The average correlation length L, extracted from the above fitting, rises from a 125-K value of 7(1) Å, which is less than the in-plane lattice parameter c, to 19(1) Å($\sim 2c$) at 40 K. Surprisingly, the average correlation length L decreased to 16(1) Å (around $1.5c$) at 6 K where partial long-range ordering has been built up. The decrease in 2D correlation length at lower temperatures is rare but reasonable in a successive partial ordering scenario as the single averaged L is likely a simplification of planar spin correlations with a continuous distribution of L's. As shown in Fig. 8(c), the fraction of scattering component with large L is identified by the relatively sharp contribution in the vicinity of the intensity maximum at $2\theta = 18^\circ$, indicating a new 3D ordering condensation initiate around 6 K. Apparently, a magnetic peak at $2\theta = 18^\circ$ will grow and become significantly stronger at the expanse of the remaining 2D ordering states below 6 K. The correlation of the low-temperature magnetic structures of this phase below 6 K invite further detailed neutron-diffraction investigations. Moreover, Fig. 9 shows a T behavior which is not critical, such as above ~26 K, the more accurate method of measuring the integrated intensity of the magnetic peaks vs T could be helpful in determining the

true critical temperature. Low-temperature neutron-scattering and density functional theory calculations may also shed light on the behaviors observed in this TLA system.

IV. CONCLUSION

To summarize, a layered geometrically frustrated insulator CaOFeS, containing alternating CaO and FeS triangular sheets, was synthesized and characterized by susceptibility, heat-capacity, electric transport, and neutron powder-diffraction measurements. The impact of the tiny impurities that appear in the compound can be safely excluded in the measured temperature ranges. Below room temperature, 2D short-range ordering within CaOFeS is inferred from a broad maximum centered at 120 K in susceptibility, a very broad magnetic specific-heat contribution, and a Warren-type broad peak in the neutron spectra. The geometrically frustrated compound condenses into a partial long-range ordered state with AFM coupled Fe layers below $T_N = 40.6$ K with the partial long-range order transition completed at 26 K. The resulting partially ordered magnetic structure is *G*-type Ising AFM with a propagation vector of $\mathbf{k} = (1/2, 1/2, 0)$ and an ordered magnetic moment of $2.59(3)\mu_B$/Fe along c at 6 K. No further structural distortion appears to accompany the 3D magnetic ordering.

ACKNOWLEDGMENTS

S. F. Jin would like to thank Dr. X. F. Lai, H. Zhang, and S. J. Shen for helpful discussions. This work was financially supported by the National Natural Science Foundation of China under Grants No. 91422303, No. 51202286, and No. 51472266.

[1] R. Moessner and A. P Ramirez, Phys. Today **59**(2), 24 (2006).
[2] K. Hirakawa, H. Kadowaki, and K. Ubukoshi, J. Phys. Soc. Jpn. **52**, 1814 (1983).
[3] S. Nakatsuji, Y. Nambu, H. Tonomura, O. Sakai, S. Jonas, C. Broholm, H. Tsunetsugu, Y. Qiu, and Y. Maeno, Science **309**, 1697 (2005).
[4] M. F. Collins and O. A. Petrenko, Can. J. Phys. **75**, 605 (1997).
[5] P. W. Anderson, Mater. Res. Bull. **8**, 153 (1973).
[6] S. E. Nagler, W. J. L. Buyers, R. L. Armstrong, and B. Briat, Phys. Rev. B **27**, 1784 (1983).
[7] W. B. Yelon, D. E. Cox, and M. Eibschutz, Phys. Rev. B **12**, 5007 (1975).
[8] M. Mekata and K. Adachi, J. Phys. Soc. Jpn. **44**, 806 (1978).
[9] S. K. Kuindersma, C. Haas, J. P. Sanchez, and R. Ai, Solid State Commun. **30**, 403 (1979).
[10] Y. Kamihara, T. Watanabe, M. Hirano, and H. Hosono, J. Am. Chem. Soc. **130**, 3296 (2008).
[11] K. Ueda, S. Inoue, S. Hirose, H. Kawazoe, and H. Hosono, Appl. Phys. Lett. **77**, 2701 (2000).
[12] H. Hiramatsu, H. Kamioka, K. Ueda, M. Hirano, and H. Hosono, J. Ceram. Soc. Jpn. **113**, 10 (2005).
[13] T. Sambrook, C. F. Smura, and S. J. Clarke, Inorg. Chem. **46**, 2571 (2007).
[14] S. A. Petrova, V. P. Mar'evich, R. G. Zakharov, E. N. Selivanov, V. M. Chumarev, and L. Yu. Udoeva, Dokl. Chem. **393**, 255 (2003).
[15] E. N. Selivanov, V. M. Chumarev, R. I. Gulyaeva, V. P. Mar'evich, A. D. Vershinin, A. A. Pankratov, and E. S. Korepanova, Inorg. Mater. **40**, 845 (2004).
[16] J. E. Greedan, N. P. Raju, and I. J. Davidson, J. Solid State Chem. **128**, 209 (1997).
[17] H. Kabbour, E. Janod, B. Corraze, M. Danot, C. Lee, M.-H. Whangbo, and L. Cario, J. Am. Chem. Soc. **130**, 8261 (2008).
[18] R. Navarro, *Magnetic Properties of Layered Transition Metal Compounds* (Kluwer Academic, Dordrecht, 1990).
[19] J. X. Zhu, R. Yu, H. Wang, L. L. Zhao, M. D. Jones, J. Dai, E. Abrahams, E. Morosan, M. Fang, and Q. Si, Phys. Rev. Lett. **104**, 216405 (2010).
[20] C. Wang, M. Q. Tan, C. M. Feng, Z. F. Ma, S. Jiang, Z. A. Xu, G. H. Cao, K. Matsubayashi, and Y. Uwatoko, J. Am. Chem. Soc. **132**, 7069 (2010).
[21] N. Ni, E. Climent-Pascual, S. Jia, Q. Huang, and R. J. Cava, Phys. Rev. B **82**, 214419 (2010).
[22] Y. Fuwa, M. Wakeshima, and Y. Hinatsu, J. Phys.: Condens. Matter **22**, 346003 (2010).
[23] N. F. Mott, Philos. Mag. **19**, 835 (1969).
[24] F. Han, X. Wan, B. Shen, and H.-H. Wen, Phys. Rev. B **86**, 014411 (2012).
[25] J. Rodríguez-Carvajal, Phys. B **192**, 55 (1993).
[26] I. Solovyev, N. Hamada, and K. Terakura, Phys. Rev. Lett. **76**, 4825 (1996).
[27] T. Sato, H. Kadowaki, H. Masuda, and K. Iio, J. Phys. Soc. Jpn. **63**, 4583 (1994).
[28] J. L. Soubeyroux, D. Fruchart, J. C. Marmeggi, W. J. Fitzgerald, C. Delmas, and G. Le Flem, Phys. Status Solidi A **67**, 633 (1981).
[29] H. Kadowaki, H. Takei, and K. Motoya, J. Phys.: Condens. Matter **7**, 6869 (1995).
[30] Y. Oohara, S. Mitsuda, H. Yoshizawa, N. Yaguchi, H. Kuriyama, T. Asano, and M. Mekata, J. Phys. Soc. Jpn. **63**, 847 (1994).
[31] E. Granado, J. W. Lynn, R. F. Jardim, and M. S. Torikachvili, Phys. Rev. Lett. **110**, 017202 (2013).
[32] B. E. Warren, Phys. Rev. **59**, 693 (1941).